Development 127, 755-767 (2000)
Printed in Great Britain © The Company of Biologists Limited 2000
DEV9690

mab-20 encodes Semaphorin-2a and is required to prevent ectopic cell contacts during epidermal morphogenesis in *Caenorhabditis elegans*

Peter J. Roy[1,2], Hong Zheng[2], Charles E. Warren[2] and Joseph G. Culotti[1,2,*]

[1]Samuel Lunenfeld Research Institute, Mount Sinai Hospital, 600 University Avenue, Toronto, Ontario M5G 1X5, Canada
[2]Department of Molecular and Medical Genetics, University of Toronto, Toronto, Ontario M5S 1A8, Canada
*Author for correspondence (culotti@mshri.on.ca)

Accepted 22 November 1999; published on WWW 26 January 2000

SUMMARY

The Semaphorins are a family of secreted and transmembrane proteins known to elicit growth cone repulsion and collapse. We made and characterized a putative null mutant of the *C. elegans* gene *semaphorin-2a* (*Ce-sema-2a*). This mutant failed to complement mutants of *mab-20* (Baird, S. E., Fitch, D. H., Kassem, I. A. A. and Emmons, S. W. (1991) *Development* 113, 515-526). In addition to low-frequency axon guidance errors, *mab-20* mutants have unexpected defects in epidermal morphogenesis. Errant epidermal cell migrations affect epidermal enclosure of the embryo, body shape and sensory rays of the male tail. These phenotypic traits are explained by the formation of inappropriate contacts between cells of similar type and suggest that Ce-Sema-2a may normally prevent formation or stabilization of ectopic adhesive contacts between these cells.

Key words: Caenorhabditis elegans, Semaphorin, mab-20, Cell contact, Adhesion

INTRODUCTION

Understanding how axon and cell migrations are guided is fundamental to our understanding of metazoan development. During directed migrations, the leading edge of growing axons and motile cells must continually establish transient contacts to neighboring cells and the surrounding extracellular matrix (ECM) via membrane extensions. It is through the modulation of the cytoskeletal network within these membrane extensions that molecular cues can guide cells to their target destination (Tanaka and Sabry, 1995; Carlier, 1998).

Simplistically, migratory guidance cues can be classified as those that attract and those that repel. There are also cues that can both attract and repel, depending on the receptor complex receiving the cue (Hedgecock et al., 1990; Leung-Hagesteijn et al., 1992; Chan et al., 1996) and the activity of signaling components downstream of the activated complex (Song et al., 1998). Attractive cues are thought to promote membrane extension towards increasing concentrations of the cue by increasing the affinity of the extension to the substratum (de la Torre et al., 1997). In contrast, repulsive cues can induce localized collapse of membrane extensions through the disassembly of microfilaments within the extensions (Fan and Raper, 1995). However, exactly how these cues regulate the cytoskeletal elements required for membrane extension and cell motility is not clear. Even less is known about the way migrating cells transiently make and break contacts with the ECM and other cells that line their migratory paths. To address these issues, we have begun a genetic analysis of semaphorin function in the nematode *Caenorhabditis elegans*.

The semaphorins are a family of guidance cues conserved from nematodes to humans. At least eight classes of semaphorins have been identified based on their overall domain composition. All have a conserved ~500 amino acid "semaphorin" domain that defines the family (Semaphorin Nomenclature Committee, 1999). The first semaphorin, Semaphorin-1a, was discovered in the grasshopper and is required for axon guidance and fasciculation (Kolodkin et al., 1992). Fan and Raper (1995) later showed that Semaphorin3A (SEMA3A) can directly steer growing axons in vitro via contact-mediated repulsion. The ability of semaphorins to repel axons in vivo is supported by studies of *Drosophila* Semaphorin-2a (D-Sema-2a). During the final stages of pathfinding, subsets of motoraxons that normally invade muscle beds are selectively prevented from doing so upon D-Sema-2a overexpression in muscle (Winberg et al., 1998). Conversely, in *D-sema-2a* mutants, certain motoraxons ectopically invade muscle beds that normally express D-Sema-2a.

Axon repulsion, however, is not the only function of the semaphorin family since some semaphorins reportedly attract growing axons (Wong et al., 1997; Bagnard et al., 1998) while others, such as D-Sema-2a and mouse Sema3A, are essential for viability (Kolodkin et al., 1993; Behar et al., 1996). Aside from neuronal defects, Sema3A mutants also have fused ribs and vertebrae, and cardiac malformations (Behar et al., 1996). Constitutive overexpression of the Sema3A receptor, neuropilin-1, also results in cardiac malformations, along with defasciculation and excessive sprouting of neurons and cardiovascular defects (He and Tessier-Lavigne, 1997;

Kitsukawa et al., 1995). In principle, the cardiovascular defects may be explained by the promiscuity of the neuropilin-1 receptor, as it also binds an isoform of VEGF (Soker at al., 1998). The mechanisms underlying the other non-neuronal defects induced by neuropilin-1 overexpression, and those of the *Drosophila* and mouse semaphorin mutants remain obscure; however, a recent report suggests that chicken SEMA3A can repel neural crest cells in vitro and possibly in vivo (Eickholt et al., 1999).

To further study semaphorin function in vivo, we used transposon-mediated reverse genetics to obtain a putative null allele of the *semaphorin-2a* gene in *C. elegans (Ce-sema-2a*). This allele failed to complement mutations in the previously uncloned *mab-20* gene (Baird et al., 1991). The mutant phenotype demonstrates that the predicted gene product Ce-Sema-2a is required for axon guidance and cell migrations. However, a major role of Ce-Sema-2a is to regulate the morphogenesis of the epidermis, historically called the hypodermis in *C. elegans*. *Ce-sema-2a* mutants exhibit several inappropriate hypodermal cell contacts during embryonic development. Mutant defects in hypodermal enclosure of the embryo, and in the morphogenesis of the body wall and the sensory rays of the male tail can be explained by these inappropriate contacts. Our results suggest that Ce-Sema-2a may play a key role in tissue morphogenesis by preventing the formation or stabilization of adhesive contacts between cells of a similar type.

MATERIALS AND METHODS

Standard molecular biology methods were used (Sambrook et al., 1989) unless otherwise noted. General procedures used for the culture, maintenance and storage of the nematodes are compiled by Wood (1988). All strains not isolated in our laboratory were obtained from the *C. elegans* Genetics Center, care of T. Stiernagle (The University of Minnesota). Primer sequences are available upon request.

cDNA construction

The λZAPII (Stratagene) cDNA clones *yk80* and *yk100* were provided by Y. Kohara and excised in vivo. To obtain the 5′ end of the cDNA, the RACE procedure was used (Frohman et al., 1988) on total RNA from a mixed stage population of wild-type nematodes (N2). First-strand cDNA was synthesized using the *mab-20*-specific primer II.RO. A polymerase chain reaction using an oligo(dT) primer and the gene-specific primer II.RI generated a 1.25 kb product from a first-strand cDNA template tailed with dATP, and was then cloned into pBluescript KS (+). A polymerase chain reaction using the splice leader sequence 1 (SL1) 5′ primer (Krause and Hirsh, 1987) and the *mab-20*-specific primer II.RI generated a 1.55 kb product, which was cloned into pBluescript KS (+). The full-length cDNA was spliced together using the SL1 PCR product's 5′ end to *Bam*HI, the 5′ RACE product's *Bam*HI-*Sma*I fragment, and *yk80* 3′ from the *Sma*I restriction site. The cDNA was sequenced in its entirety.

The *evCe-sema-2a* cDNA was released from its vector using polylinker sites *Xba*I and *Xho*I, and used to probe a northern blot of 5 μg of total RNA from a mixed-stage population of wild-type nematodes (N2), prepared as described in Leung-Hagesteijn et al. (1992).

Genomic clones

1.3×10^6 plaques from an Embl3 genomic phage library were screened using a 1.25 kb *evCe-sema-2a* cDNA fragment released from its vector using the *Eco*RI cDNA restriction sites. One of ten positive isolates, *evpZH13*, contained the predicted *mab-20* gene in its entirety. A subclone of this phage isolate, *evpPRII.2*, was demonstrated, by restriction analysis, sequencing and transgenic rescue of the mutant, to contain an entire functional *mab-20* gene. The transcriptional fusion reporters *evpPRII.67* and *evpPRII.75* were constructed by inserting 2.5 kb of DNA 5′ to the predicted initiator methionine of *mab-20* inserted into the GFP vectors *pPD95.67* and *pPD95.75*, respectively. The translational fusion reporter *evpPRII.14* was constructed by inserting in frame the GFP-coding sequence and introns contained within a 1.1 kb *Eco*RI fragment of DNA excised from *pPD95.85* into the fourth *Eco*RI site of *evpPRII.2*. The *pPD* series of vectors were a gift from A. Fire.

Screening for Tc1 alleles and deletion derivatives

The strategy for the construction of our Tc1 library is an extension and modification of previous work (Zwaal et al., 1993) and is detailed in Roy (1999). Alpha-pool DNA was screened for an insertion allele in *mab-20* using nested PCR with gene-specific primers II.A and II.B and Tc1-specific primers. AmpliTaq Gold™ (Perkin-Elmer) was used in all PCR reactions. To obtain a deletion allele of *mab-20*, a sublibrary was constructed and screened in the same fashion as the original, with the exception of using NW1034 *[mab-20(ev573::Tc1); mut-2(r459); dpy-19(n1347)]* as the founding strain. To screen the alpha-pools of the sublibrary, PCR was carried out using *mab-20*-specific primers II.Y, II.Z, II.9, and II.10. The resulting *mab-20(ev574)* allele was outcrossed with N2 or *him-5(e1490)* at least 11 times before being analyzed further.

Genetic linkage and complementation

From *ev574*/+; *dpy-5(e61)*/+ double heterozygotes, 115 Dpy animals were picked that had no morphological defects like those of *ev574* homozygotes. Only 23 of these clones threw *ev574* homozygous progeny, showing loose linkage to *dpy-5* on chromosome I, as is also true for *mab-20* mutants, which have similar phenotypes. *mab-20(bx61^{ts}); him-5(e1490)* males raised at the permissive temperature (16°C) were mated with *ev574* hermaphrodites. Male cross progeny raised at 25°C were scored for ray fusions. Since neither *mab-20(bx24)* nor *mab-20(ev574)* male homozygotes can successfully mate, the complementation test between these two alleles was done by crossing *mab-20(bx24)*/+ males to *mab-20(ev574)* hermaphrodites. All male cross progeny were scored for ray fusions. Since no deficiency uncovers the *mab-20* locus, the supposition that *ev574* is a genetic null cannot be tested.

Transgenics

Extrachromosomal arrays of *Ex[mab-20(+)(evpPRII.2); rol-6(su1006)]* were generated by co-microinjection of the DNAs into N2 oogonia (Mello and Fire, 1995) at a concentration of 27.5 ng/μl and 100 ng/μl, respectively. F_1 and F_2 transformants were selected based on the dominant rolling phenotype induced by *rol-6(su1006)*. The extrachromosomal arrays were integrated into random double-stranded breaks in the chromosomes generated by 3000 rads from a ^{137}Cs source, resulting in intrachromosomal arrays *evIs74a*, *evIs74b*, *evIs74c* and *evIs74d*. Similar procedures were used to create reporter arrays.

Microscopy

Male tail ray fusions, ventral enclosure defects and DTC migratory defects were scored by mounting 1 mM levamisole-treated animals on 2% agarose pads for observation using DIC optics (Leica DMR microscope). The *mec-4::gfp* reporter (a gift from M. Driscoll) was used to asses the migrations of QL and QR. The migration of QL was considered aberrant if the PVM was situated near or anterior to the vulva.

For whole-mount immunohistochemistry, animals were permeabilised as described by Finney and Ruvkun (1990), and incubated overnight at room temperature with mAbMH27 or anti-

Table 1. Male tail sensory ray fusions

Genotype	°C	R1	R2	R3	R4	R5	R6	R7	R8	R9	>2R	*n*	Notes
control	RT	0	0	0	0	0	0	0	4	4	0	317	
mab-20(ev574)	RT	92	99	97	96	3	63	92	12	93	87	200	
mab-20(ev574)	25	88	98	99	97	3	61	91	8	90	94	120	
mab-20(ev574)/+	RT	0	0	1	2	0	1	0	3	3	0	170	*ev574* is recessive
mab-20(bx24)	RT	69	83	96	90	1	25	41	2	41	43	200	*ev574* does not
mab-20(ev574)/mab-20(bx24)	RT	85	98	97	98	4	63	90	14	89	92	119	complement *bx24*
mab-20(bx61)	16	2	7	50	48	0	0	7	0	7	2	245	*bx61* is temperature
mab-20(bx61)	RT	17	23	55	53	0	1	16	7	19	10	100	sensitive and
mab-20(bx61)	25	12	22	94	91	0	2	14	1	14	9	170	*ev574* does not
mab-20(ev574)/mab-20(bx61)	25	25	73	97	94	0	5	57	2	54	50	125	complement *bx61*
mab-20(ev574); evIs74c	RT	2	3	2	0	0	0	6	0	6	0	124	*ev574* is rescued by
mab-20(ev574); evIs74d	RT	1	1	0	0	0	0	0	2	2	0	243	*evIs74c* and *evIs74d*

The body of the table gives the percentage of ray fusion to a neighbor within one side of a male tail (animals grown at 23ºC). The column heading '>2R' refers to the percentage of male tail sides that had more than two rays within a single fusion. *evIs74a-d* represent a series of four independently isolated transgene arrays of genotype *[mab-20(+) (evpPRII.2); rol-6(su1006)]* that are derived from the chromosomal integration of the same extrachromosomal array *evEx74*. *evIs74a* and *evIs74b* more closely phenocopy *mab-20* mutant phenotypes and contain more copies of *mab-20(+)* than *evIs74c* or *evIs74d* (data not shown). All strains contained *him-5(e1490)*.

LIN-26 antibodies. The next day the animals were incubated with FITC-conjugated goat secondary antibody (Sigma™).

Circumferential microfilaments were observed by fixation in 4% paraformaldehyde and 0.5% glutaraldehyde, followed by a brief 5 minute exposure to rhodamine-conjugated phalloidin and 0.2% Triton X-100 (Priess and Hirsh, 1986). Although this procedure is intended for viewing the circumferential microfilaments, sarcomeric microfilaments were sometimes observed and cell outlines were visible.

SEM analysis of embryos was carried out according to the methods of Williams-Masson et al. (1997), except that specimens were coated with 1-2 nm of gold and observed with a JOEL 820 scanning electron microscope.

The numerous short-range migrations and rearrangements of wild-type seam cells and their precursors during the creation of the seam was observed through the use of the demonstration version of the BioCell CD ROM ™, freely available from R. Schnabel (Schnabel et al., 1997).

RESULTS

Cloning of the *C. elegans semaphorin-2a* gene

A *C. elegans* gene (corresponding to yac Y54E5B.1 on linkage group I) predicted to encode a semaphorin-1 homolog (Ce-Sema-1a) was initially cloned using degenerate oligonucleotides and sequenced (Roy, 1999). This sequence was used to search the *C. elegans* genome database using the BLAST program (Altschul et al., 1994). Two additional semaphorin genes (D1037.2 and Y71G12A_205.G) also on linkage group I were identified. D1037.2 encodes another semaphorin-1 homolog (Ce-Sema-1b) while Y71G12A_205.G encodes a semaphorin-2 homolog (Ce-Sema-2a). Here we focus on the mutagenesis and characterization of the *semaphorin-2a* gene as it produces more severe defects than mutations in the *semaphorin-1* related genes (P. J. R., V. Ginzburg and J. G. C., unpublished results).

A 2.4 kb *evCe-sema-2a* cDNA (Fig. 1) was isolated and used to probe a northern blot of mRNA purified from a mixed-stage population of wild-type (N2) worms. This reveals a single RNA species of approximately 2.4 kb (data not shown). The *evCe-sema-2a* cDNA is predicted to encode a 657 amino acid protein, consisting of an amino-terminal hydrophobic signal sequence, followed by a semaphorin domain, a C2-type immunoglobulin domain, and a non-conserved carboxy-terminal region (Fig. 1). This modular configuration is the same as that predicted for *Drosophila* Sema-2a (Kolodkin et al., 1993) which is 32% identical and 41% similar to Ce-Sema-2a and conserves 17 of the 19 cysteines of Ce-Sema-2a. The semaphorin domain of Ce-Sema-2a has 13 of the 14 conserved cysteines that define this domain.

The *evCe-sema-2a* cDNA was used to isolate a 15.4 kb genomic lambda phage clone. A 14.6 kb subclone of this phage, *evpPRII.2* (Fig. 2), rescues a putative null *Ce-sema-2a* mutation *(ev574)*, suggesting that the subclone contains all elements required for proper functioning of the *Ce-sema-2a* gene (Table 1).

The isolation and molecular characterization of a *C. elegans sema-2a* mutant

A *Ce-sema-2a* silent transposon-insertion mutant, strain NW1034 [*Ce-sema-2a(ev573::Tc1)I, mut-2(r459)I; dpy-19(n1347)III*], was obtained by PCR screening of a frozen library of worms containing active Tc1 transposons. NW1034 was propagated and screened for a deletion derivative of *ev573::Tc1*, resulting in the isolation of NW1074 [*Ce-sema-2a(ev574)*]. PCR, Southern analysis and sequencing show that *ev574* contains a deletion of 1479 bp that includes part of the first intron, the entire first exon, and 641 bp 5′ to the predicted initiator methionine, thereby eliminating the predicted signal sequence (Fig. 2). As no other methionine is present until residue 120, *ev574* is predicted to be a molecular null allele of *Ce-sema-2a*.

NW1074 worms are deformed (see Fig. 4), a trait that maps to linkage group I (see Materials and Methods). Concurrent with mapping studies, phenotypic analysis of *ev574* homozygotes revealed that the normally distinct sensory rays of the adult male tail are fused, a phenotypic trait referred to as Mab, or male abnormal (see Fig. 5). The fusion pattern is similar to that observed in mutants of *mab-20* on linkage group

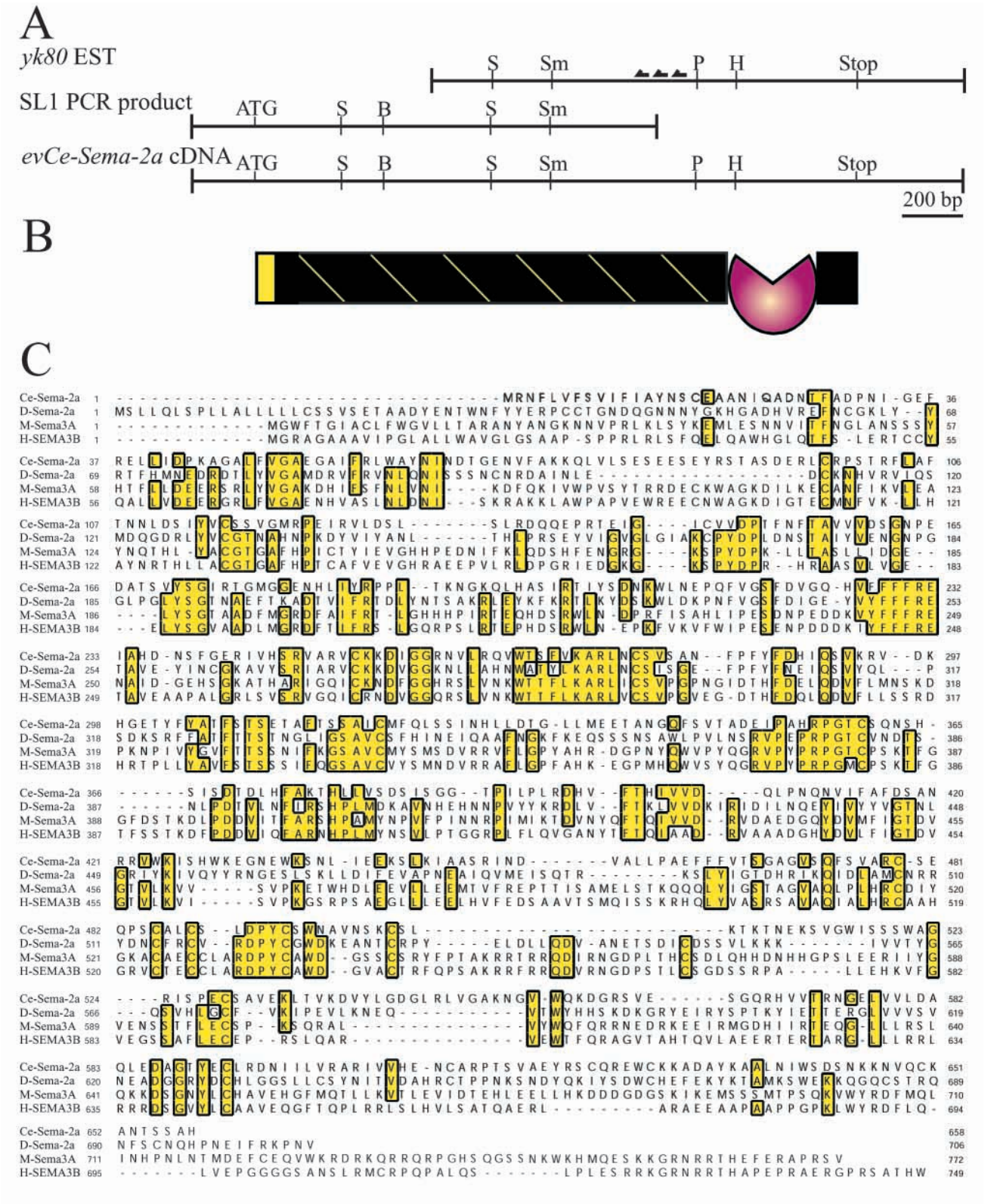

I (map position –10.4; Baird et al., 1991). Genetic crosses revealed that *ev574* does not complement *mab-20(bx24)* or *mab-20(bx61)* (Table 1), suggesting that *mab-20* encodes Ce-Sema-2a.

SSCP, PCR, Southern and DNA sequence analyses revealed that *bx24* is an internal, out-of-frame, tandem duplication of a 2.2 kb sequence normally found immediately 5′ to the predicted stop codon of *Ce-sema-2a* (Fig. 2). The temperature-sensitive allele *bx61* is a missense mutation that changes the 188th codon from a proline to a leucine. The nature of the three mutations is consistent with the relative penetrance of all of the phenotypic traits of the three *mab-20* alleles examined, which

Fig. 1. The isolation, construction and predicted protein sequence of the *C. elegans Semaphorin-2a* cDNA. (A) Construction of the full-length *Semaphorin-2a* cDNA. The sequence of *yk80* (a gift from Y. Kohara) was used to design primers (arrows) to produce a 5′ RACE product (not shown) and an SL1 PCR product. The *Sma*I site was used to splice the clones together to produce a full-length clone, *evCe-Sema-2a*, which was sequenced. Restriction sites: S, *Sal*I; Sm, *Sma*I; P, *Pst*I; H, *Hin*dIII; B, *Bam*HI; ATG, predicted translational start; Stop, stop codons. (B) The predicted 658 amino acid protein product of *evCe-Sema-2a* with signal sequence (yellow box), semaphorin domain (hatched box) and Ig domain (3/4 circle). (C) A multiple sequence alignment shows conserved residues in Ce-Sema-2a. The alignment includes *C. elegans* Semaphorin-2a (Ce-Sema-2a, accession number AF216968); *Drosophila* Semaphorin-2a (D-Sema-2a, Kolodkin et al., 1993, accession number L26083); mouse Semaphorin3A (M-Sema3A, Puschel et al., 1995, accession number X85993); and Human Semaphorin V (H-SEMA3B, Sekido et al., 1996, accession number U28369). Conserved residues are boxed. Residues predicted to be missing in *mab-20(ev574)* are shown in bold.

can be placed into a simple allelic series (Table 1). The *Ce-sema-2a* gene is hereafter called *mab-20*, and the predicted protein product Ce-Sema-2a or simply Sema-2a.

mab-20 mutants have ventral enclosure defects

Initial observations of *mab-20* mutants suggested that hermaphrodites have a low fecundity, a defect that is rescued zygotically upon the introduction of *mab-20*(+) either by mating or as a transgene (data not shown). In a given population, 84% (*n*=452) of *mab-20(ev574)*; *him-5(e1490)* embryos die, apparently from the extrusion of internal contents from the ventral side during the elongation phase of development (Fig. 3A,B). The embryonic lethality of *ev574* is rescued by a *mab-20*(+) transgene array; only 28% (*n*=256) of *mab-20(ev574)*; *evIs74d [mab-20(+) (evpPRII.2); rol-6(su1006)]; him-5(e1490)* embryos die. Incomplete rescue is attributed to the lethality conferred by the integrated *evIn74d* array; 40% (*n*=235) of *evIs74d; him-5(e1490)* embryos die, most from the extrusion of internal contents. In addition, 15% (*n*=223) of *him-5(e1490)* control embryos die for unknown reasons, a result that has been repeated with several isolates of *him-5(e1490)*. Interestingly, *mab-20* mutant embryos burst at the ventral midline in a manner similar to animals mutant for the VAB-1 Eph receptor tyrosine kinase (Fig. 3C). *vab-1* mutants are thought to burst because of a failure to properly enclose the ventral surface with hypodermis (George et al., 1998). These observations prompted an investigation of ventral enclosure of *mab-20(ev574)* mutant embryos. The process of ventral enclosure is reviewed below.

By 250 minutes after first cleavage in wild-type animals, two dorsal, two lateral and two ventral rows of hypodermal cells are aligned longitudinally and sit on the embryo in a dorsal-posterior locale, leaving the ventral blast cells exposed (Podbilewicz and White, 1994). The ventrally directed migration of the hypodermis is led by two anterior pairs of ventral hypodermal cells on either side of the embryo called leader cells. Of all ventral hypodermal cells, only the leader cells have been reported to extend substantial actin-filled membrane extensions toward the ventral midline (Fig. 3D; Williams-Masson et al., 1997). After the contralateral leader cells meet and form junctions at the ventral midline, the trailing posterior ventral hypodermal cells, called pocket cells, leave a ventral pocket of neuroblasts uncovered (see Fig. 3G). A microfilament purse-string mechanism is thought to draw the pocket cells together and complete hypodermal enclosure of the embryo (Williams-Mason et al., 1997). Twelve of the seventeen pocket cells are P neuroectoblasts (P cells) and are arranged in two longitudinal rows of six cells each (Podbilewicz and White, 1994). After enclosure, all ventral hypodermal cells fuse into either the hyp6 or hyp7 hypodermal syncytium except for the six pairs of P cells. The dorsal side of each of the twelve rhomboid P cells contacts two lateral hypodermal cells, called

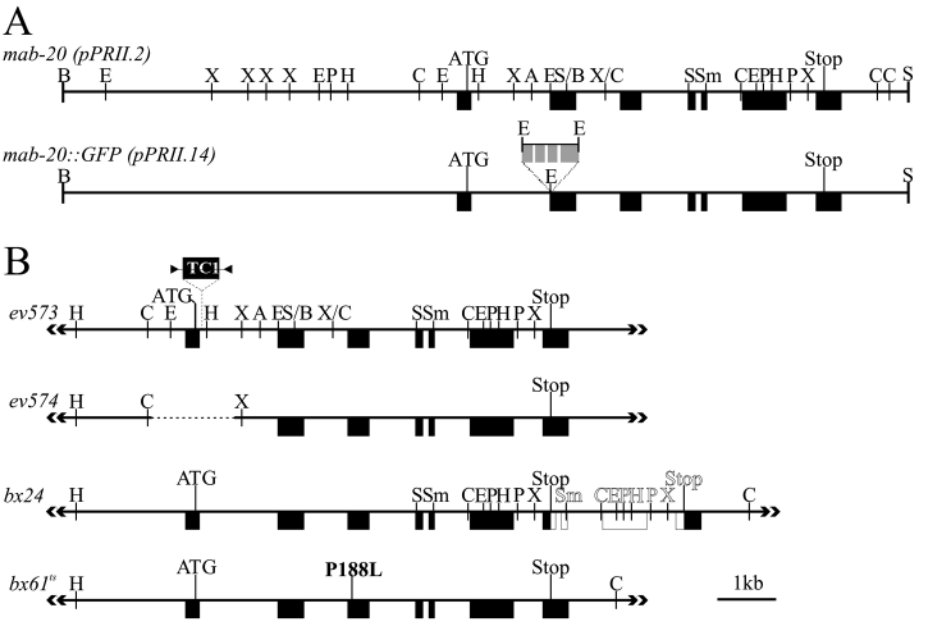

Fig. 2. Genomic subclones and *mab-20* alleles. (A) Restriction map of the 14.6 kb genomic *mab-20* subclone *evpPRII.2*. The *mab-20* reporter construct, *evpPRII.14*, is a translational fusion to GFP, which is inserted into the 35th codon of Ce-Sema-2a. (B) Four alleles of *C. elegans mab-20*. *ev573::Tc1* contains a transposon inserted after nucleotide +103 of the coding sequence. *ev574* is a 1.5 kb deletion predicted to remove the amino-terminal 25 amino acids of Ce-Sema-2a. *bx24* contains an internal tandem duplication of 2.2 kb that is predicted to remove the last residue of Ce-Sema-2a and add 26 residues of gibberish. *bx61*^{ts} has a cytosine to thymine change leading to a predicted leucine substitution for proline at residue 188. Restriction sites: S, *Sal*I; Sm, *Sma*I; E, *Eco*RI; H, *Hin*dIII; X, *Xba*I; C, *Cla*I; A, *Asp*718; B, *Bam*HI; P, *Pst*I; ATG, predicted translational start codon; Stop, stop codons. Black boxes represent exons; shaded boxes represent exons of *gfp*. White boxes and restriction sites in *bx24* represent the tandem duplication.

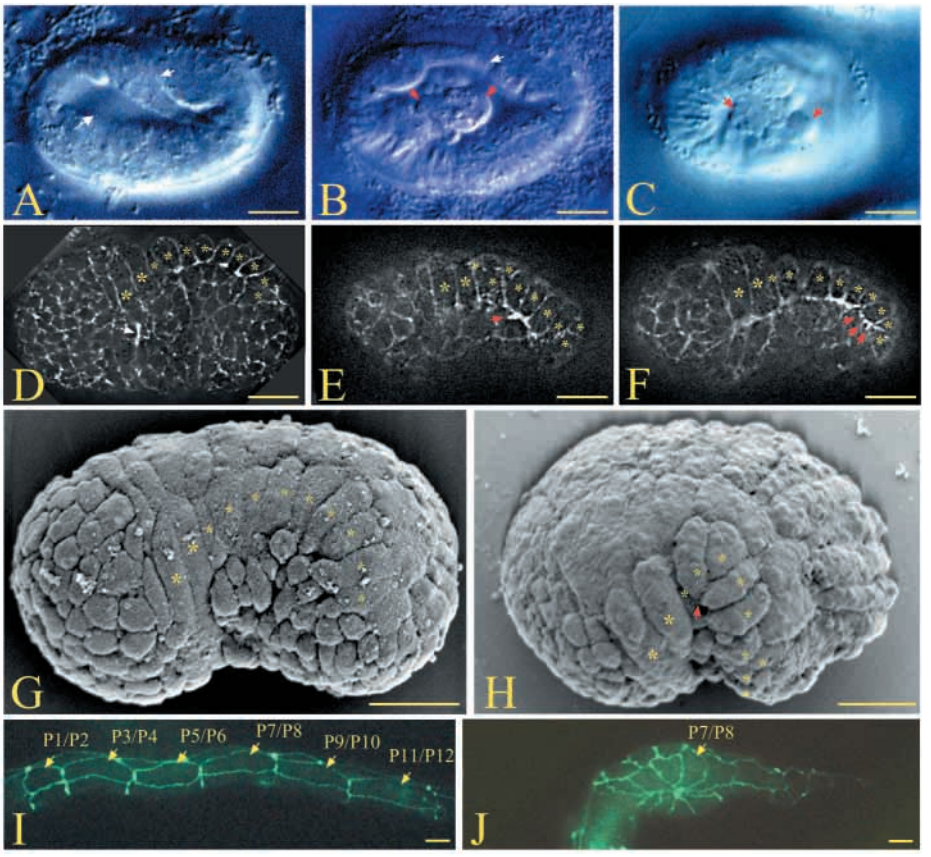

Fig. 3. Ventral enclosure defects of *mab-20* mutants are associated with ectopic pocket cell contacts. (A-C) DIC photomicrographs of control (A), a *mab-20(ev574)* (B), and a *vab-1(e2027)* (C) embryo at approximately the threefold stage of development. In *mab-20(ev574)* and *vab-1(e2027)* animals, internal contents (red arrows) have extruded from the ventral midline. Where visible, heads and tails are indicated with long or short white arrows, respectively. (D-J) Animals from a ventral-lateral perspective. Anterior is to the left. (D-F) Deconvolved images of phalloidin-stained embryos with ventral hypodermal leader cells (large asterisks) and pocket cells (small asterisks) migrating toward the ventral midline (down). The leading edges of these migrating cells are actin-rich relative to other parts of the submembranous cytoskeleton. (D) A control embryo extending an actin-rich process (arrow) from a leader cell toward the ventral midline. (E,F) *mab-20(ev574)* embryos in which the pocket cells also have substantial actin-rich processes, but unlike leader cell processes do not extend towards the midline (red arrows). Note that, in F, the pocket cell that extends many processes also ectopically contacts a non-neighboring anterior pocket cell. The leader cell extensions are not affected in the mutant. (G,H) Scanning electron micrographs of a control (G) and a *mab-20(ev574)* (H) embryo during ventral enclosure showing leader cells (large asterisks) and pocket cells (small asterisks). Ectopic contacts between pocket cells (red arrowhead) are clearly visible in the mutant and may result in the obvious kink of the embryo. In both panels, neuroblasts fill the pocket ventral to the migrating leading edge hypodermal cells. (I,J) Control (I) and *mab-20(ev574)* (J) hatchlings stained for hypodermal cell boundaries with the MH27 antibody. The six P neuroectoblasts on the left side of the wild-type animal (P1/P2 etc.) are surrounded by the hypodermal syncytium, hyp7. The *mab-20(ev574)* animal exhibits a starburst pattern of P cells with numerous ectopic contacts to non-neighboring cells at the midline. Only the P7/P8 cell is labeled for reference in J. All animals shown carry the *him-5(e1490)* mutation. Scale bars are 10 μm.

seam cells, while the ventral side contacts one homologous contralateral P cell. Each P cell contacts a flanking ipsilateral P cell at each of its anterior and posterior borders, except for cells at the periphery of the P cell queue which contact a flanking P cell at one end and hyp7 at the other.

Embryos fixed and stained with rhodamine-conjugated phalloidin reveal a high density of microfilaments in the leading edge of ventral hypodermal cells that migrate towards the ventral midline (Fig. 3D-F). Actin-rich membrane extensions are observed on the leader cells of wild-type embryos, but never on pocket cells (Fig. 3D). In contrast, similar membrane extensions emanate from both leader cells and pocket cells in *mab-20(ev574)* mutants (Fig. 3E,F). Scanning electron microscopy (SEM) of embryos at the same stage of enclosure reveal ectopic contacts between the pocket cells of *mab-20(ev574); him-5(e1490)* mutants. Ectopic contacts are not observed in *him-5(e1490)* controls (n>10; Fig. 3G,H). The abnormal pocket cell extensions observed in *mab-20* mutants may be responsible for the inappropriate pocket cell contacts observed by SEM.

The SEM analysis predicts that those embryos that survive enclosure and elongate might exhibit vestigial ectopic pocket cell contacts. 78% of the mutant embryos have P cells that contact non-neighboring P cells (n=100), as determined by immunostaining with mAbMH27, which recognizes a component of adherens junctions of epithelia (Francis and Waterston, 1991). The ectopic contacts often result in a starburst pattern of cell junctions (Fig. 3I,J). No wild-type animals have ectopic P cell contacts (n=100), while only one *vab-1(e2027)* mutant was observed to have an ectopic P cell contact (n=100). Although both *vab-1* and *mab-20* mutant embryos burst from the ventral side during elongation, the underlying cellular defects responsible for this trait are apparently different in the two mutants.

The abnormal body shape of *mab-20* mutants may be caused by the misalignment of circumferential microfilaments during embryonic elongation

The most obvious phenotype of *mab-20(ev574)* homozygotes is the severe deformities in body size and shape (Fig. 4A,B). Newly hatched animals are shorter than the wild type and frequently have bulges and constrictions randomly about the body and head. This phenotypic trait is first observed after embryonic elongation begins. Approximately 88% of larvae have obvious morphological defects, compared to none for wild-type and *mab-20*(+) rescued lines. Many of the larvae

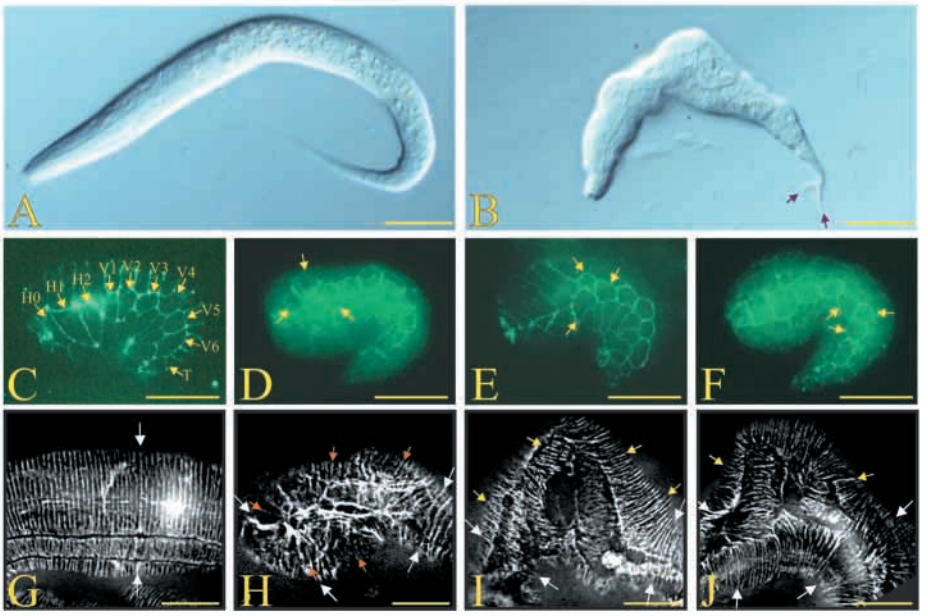

Fig. 4. The abnormal body shape of *mab-20* mutants may be caused by contraction of misaligned microfilaments during elongation. In all panels except H, animals are shown from a lateral perspective. Anterior is to the left and dorsal is up. DIC micrographs of L1 larvae illustrate that compared to control animals (A), *mab-20(ev574)* mutants (B) are shorter and have severe body morphology defects, sometimes including a split tail (arrows). (C-F) Embryos at the one and a quarter to one and a half-fold stage stained for hypodermal cell boundaries with the MH27 antibody. Hypodermal seam cells are arranged in a longitudinal queue along the lateral line of the control embryo (C), but appear clustered (yellow arrows) in various regions of *mab-20(ev574)* mutants (D-F). Note that in E, ectopic P cell contacts can also be seen on the ventral side. (G-J) Rhodamine-conjugated phalloidin-stained embryos at approximately the threefold stage. The white arrows in each panel indicate an axis perpendicular to the anterior-posterior axis, referred to here as the circumferential contour. In the control (G), hypodermal microfilaments are aligned in parallel with each other and the circumferential contour. (H) A ventral view of a *mab-20(ev574)* animal with clustered P cells that are discerned by the intense phalloidin-stain around cell perimeters. The path of visible microfilaments rarely deviates from the circumferential contour (orange arrows). (I,J) Two *mab-20(ev574)* mutant embryos with misaligned microfilaments within clustered seam cells. The yellow arrows in I and J indicate the path of microfilaments that begin on one side of the animal and are contiguous with misaligned microfilaments within seam cells. The path of microfilaments either brings them to the same side as their origin (I) or ends at a seam-to-seam cell junction (J). In either case, the path of these microfilaments does not make it from the dorsal to the ventral side. In addition, the misaligned microfilaments in both I and J are spatially coincident with the large bulge of the body wall, typical of *mab-20* mutant embryos. All strains contain *him-5(e1490).* Scale bars are 20 μm.

either outgrow the phenotype or fail to survive, leaving only 55% of adults with body deformities.

We investigated the arrangement of hypodermal cells during embryonic elongation in detail since the defects in body shape first appear during this phase. Immediately preceding elongation, bundles of parallel microfilaments align along the entire circumference of the body wall (Priess and Hirsh, 1986), which will be referred to here as the circumferential contour. The bundled microfilaments connect opposite sides of each hypodermal cell and are situated near the apical surface. Following ventral enclosure, a threefold circumferential constriction of the microfilaments results in a fourfold elongation of the embryo with no increase in cell number or volume. The force generated by the microfilaments during elongation is evenly distributed across the surface by both the embryonic sheath and hypodermal microtubules, without which animals develop bulges and constrictions (Priess and Hirsh, 1986). In principle, an altered arrangement of the hypodermal microfilaments could affect the distribution of force on the body wall and create similar bulges and constrictions.

In addition to the ectopic contacts between ventral pocket cells described above, mAbMH27 staining of embryos revealed that the lateral hypodermal seam cells also make ectopic contacts (Fig. 4C-F). 56% of *mab-20(ev574)* mutant embryo sides exhibit a disorganized row of seam cells in which at least one cell makes contacts to more than two neighboring seam cells (n=208), compared to 2% for wild-type sides (n=200). The ectopic contacts are apparent prior to elongation and persist thereafter. Intriguingly, the pattern of seam cell clusters in *mab-20* mutants is strikingly similar to earlier stages of wild-type development when the 10 seam cells on each side of the embryo are forming a lateral line. During this process, the seam cells and/or their precursors undergo numerous short-range migrations and rearrangements (see Materials and Methods; Schnabel et al., 1997). The conformation of the *mab-20(ev574)* seam cell clusters is consistent with an early arrest in the migrations of the seam cells as they form the lateral line.

We postulated that the altered P cell and seam cell hypodermal arrangements in *mab-20* mutants might be associated with alterations in microfilament alignment. To address this hypothesis, embryos were stained with rhodamine-conjugated phalloidin (Fig. 4G-J). Surprisingly, the alignment of microfilaments within pocket cells in *mab-20(ev574)* embryos deviates little from the wild type (Fig. 4H). The most striking defect is microfilament misalignment within clustered seam cells. Several extreme examples were observed in which microfilament arrays were U-shaped within the clustered seam cells, extending back toward the same side of the animal as the side of their origin (Fig. 4I). Bulges along the embryos were observed only in areas where microfilaments within neighboring seam cells were aligned obliquely with respect to the circumference. Bulges were not observed in animals that had normal seam cell arrangements.

mab-20 is required to prevent the fusion of male tail sensory rays

A third phenotypic trait that involves clustering of epidermal

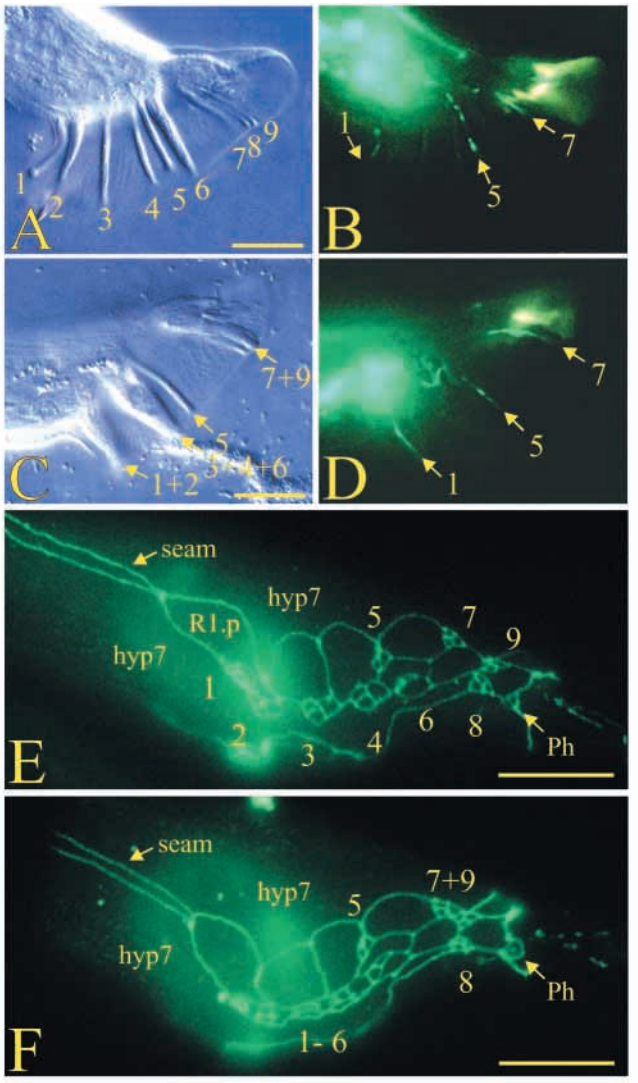

Fig. 5. *mab-20(ev574)* males have fused sensory rays. In all panels, anterior is to the left and dorsal is up. (A,C) DIC photomicrographs of the left side of control and mutant *mab-20(ev574)* adult male tails, respectively. Both lines are transgenic for *evIs82b [unc-129^{ns}::gfp(evpAC12); dpy-20(+)]*. (B,D) The corresponding fluorescence images of the male tails shown in A and C, respectively. *unc-129^{ns}*:GFP is expressed in a single neuron in each of rays 1, 5, and 7 in the control (B) and mutant (D) animals. Ray 8, anterior to the fusion of 7 and 9, is not labeled. (E,F) Control and mutant *mab-20(ev574)* larval male tails, respectively, stained for hypodermal cell boundaries with mAbMH27. Each control ray precursor cluster is distinct and appropriately labeled (E), but in the mutant, clusters 1, 2, 3, 4 and 6, as well as clusters 7 and 9 appear as indistinct aggregates (F). For reference, one R(n).p cell, R1.p is labeled in the control (E). The hypodermal syncytium (hyp7), the seam, and the phasmid socket (Ph) are indicated. All animals contain *him-5(e1490)*. Scale bars are 10 μm.

cells of a similar type is observed in *mab-20* mutant male tails. The adult male tail is a specialized structure used for copulation. It is bilaterally symmetric and each side has nine sensory rays that project laterally and are embedded within a cuticular spade-shaped fan (Fig. 5A). The ectodermal development of the male tail has been described in detail by Sulston et al. (1980) and is summarized here. Differences in the male and hermaphrodite hypodermal lineage manifest early in the third larval stage (Sulston and Horvitz, 1977). Extra rounds of division in the posterior seam cells results in 9 R(n) cells on each side, each of which gives rise to five or six cells and one programmed cell death. Two or three of the cells within each group fuse to either the surrounding hyp7, or the tail seam. The remaining three cells become a ray precursor cluster (see Fig. 5E) that develops into two neurons and a structural-support cell that ensheathes the dendrites of the two neurons. During the anterior retraction of the entire tail at the end of the fourth larval stage, the nine ray clusters remain attached to the cuticle and become surrounded by hyp7, forming the finger-like rays of the adult.

mab-20(ev574) mutant male tails have fusions of sensory rays 1 through 4, 4 with 6, and 7 with 9, a phenotypic trait that is completely rescued by *mab-20*(+) transgenes (Fig. 5C, Table 1). Baird et al. (1991) visualized cell positions during male tail morphogenesis by staining adherens junctions with mAbMH27 and showed that ray precursor clusters remain distinct in the wild type but not in *mab-20(bx24)* and *mab-20(bx61)* mutants. We compared the positions of the wild-type ray precursors to those of *mab-20(ev574)* mutants (Fig. 5E,F). Consistent with the ray fusions of *mab-20(ev574)* adults, aggregations of ray precursor clusters 1 through 4, 4 with 6, and 7 with 9 were observed by staining with mAbMH27. Clusters 5 and 8 develop in isolated locales relative to other ray clusters in the wild type and rarely fuse to other clusters in *mab-20* mutants.

A model proposed to explain why rays fuse is that each ray expresses a particular identity (Baird et al., 1991; Chow and Emmons, 1994) and that, in some mutants with fusions, ray identities equivocate. In a wild-type genetic background, the *unc-129^{ns}*::GFP reporter is highly expressed in one neuron in each of rays 1, 5 and 7. *mab-20(ev574)* mutants carrying the reporter transgene showed no difference in this expression pattern (Fig. 5B,D). In fusions involving ray 1 or 7 (ray 5 rarely fuses), only the most anterior neuron in the fusion expressed the reporter at high levels. Consistent with the finding that *mab-20* mutations confer no changes in hypodermal identity (Roy, 1999) as judged by the normal expression of the hypodermal marker LIN-26 (Labouesse et al., 1996), these results suggest that Ce-Sema-2a does not specify the identity of ray precursor clusters. Instead, Ce-Sema-2a may act to prevent the formation or stabilization of ectopic contacts between related cells of neighboring ray precursor clusters.

mab-20 mutants have defects in axon guidance and cell migration

The DA and DB motor neurons were examined for axon guidance defects in the *mab-20* mutants using an *unc-129* neural-specific (*unc-129^{ns}*::GFP) reporter (Colavita and Culotti, 1998; Colavita et al., 1998). The cell bodies of these neurons reside in the ventral cord and extend dendrites longitudinally along the ventral nerve cord and axons circumferentially to and then along the dorsal nerve cord (Fig. 6). The axons and dendrites are normally tightly fasciculated within the cords and rarely, if ever, have errant circumferential pioneer guidance defects in control animals (Table 2). 17% of *mab-20(ev574)* mutants, however, have fasciculation defects and an additional 4% have pioneer guidance defects of at least one of the DA or DB motor axons (Table 2; Fig. 6).

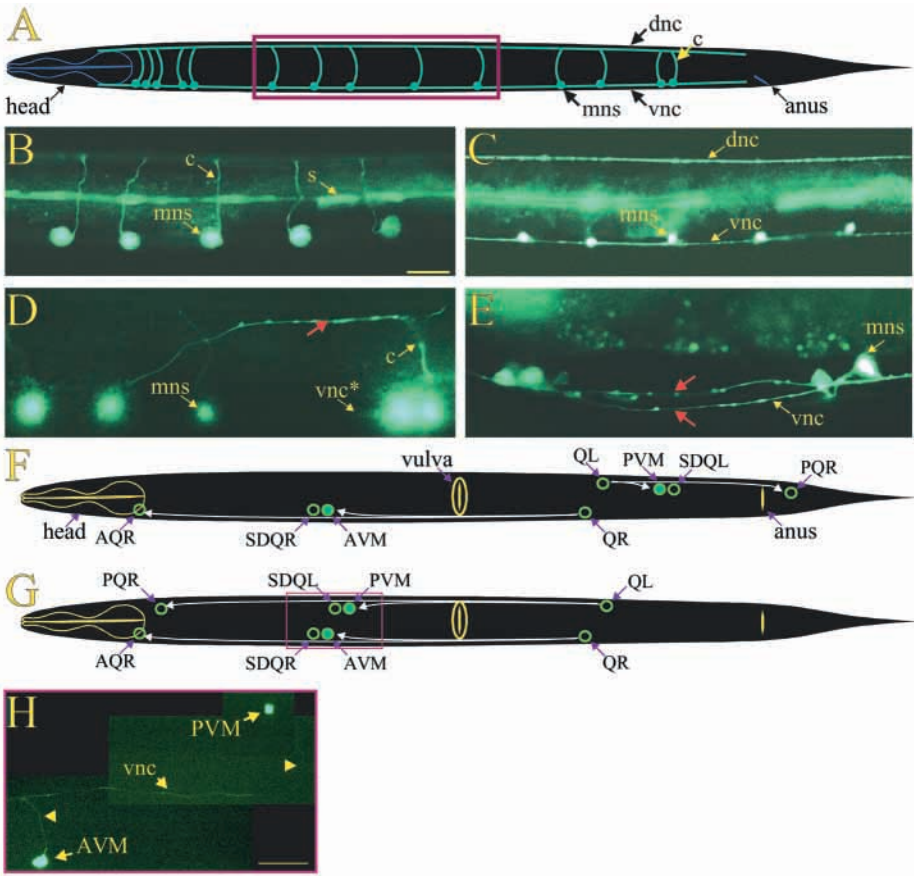

Fig. 6. *mab-20(ev574)* animals have axon and cell migration defects. (A-E) Lateral perspectives of animals that contain the transcriptional reporter *evIs82b [unc-129^{ns}::gfp (evpAC12); dpy-20(+)]* as a transgenic array. (A) Schematic of DA and DB motorneurons that express *unc-129^{ns}*::GFP showing commissures (c), dorsal nerve cord (dnc), ventral nerve cord (vnc), and motorneuron soma (mns) within the ventral nerve cord. The boxed region is shown in B to E. (B,C) *unc-129^{ns}*::GFP expresses in the DA and DB motorneuron soma (mns) in the ventral nerve cord (vnc) (in focus in C), in the DA and DB commissural axons (c) as they extend to the dorsal nerve cord (dnc) (in focus in C), and in the lateral seam cells (s). (D) Some *mab-20(ev574)* animals have at least one DA or DB commissural axon that extends to an abnormal lateral position (red arrow) and does not reach the dorsal nerve cord. (E) Some *mab-20(ev574)* animals have fasciculation defects (red arrows) in the ventral nerve cord (vnc), the dorsal nerve cord (not shown), or both (see Table 2). (F-H) shows ventral perspectives of animals that contain the transcriptional reporter *mec-4::gfp*, which is expressed in the six touch neurons, AVM, ALMR, ALML, PVM, PLMR and PLML. Only the AVM and PVM (green-filled) are progeny of the Q cells (outlined in green). (F) A schematic of Q cell and Q cell progeny migrations in the wild type. (G) A schematic of Q cell and Q cell progeny migrations in *mab-20* mutants. The box delimits the area shown in H. (H) A photomicrograph composite of a representative *mab-20(ev574); mec-4::gfp* animal showing a PVM cell body displaced to a position just posterior of AVM (axons indicated with arrowheads). Scale bars are 20 μm.

In addition to the axon guidance defects, *mab-20* mutants have ectodermal and mesodermal cell migration errors. Occasionally, the left Q neuroblast (QL) and the distal tip cells (DTCs) fail to stop migrating at typical positions in *mab-20(ev574)* mutants. QL normally undergoes a short posterior-oriented migration then divides. Its posterior daughter normally stops migrating and gives rise to the PVM touch receptor neuron (reviewed in Hedgecock et al., 1987). The total migratory distance of QL is less than 1 epithelial cell diameter, leaving PVM in the posterior quarter of the animal. PVM was found near or anterior to the mid-body in 27% of *mab-20* animals (n=184) compared to 0% for wild-type controls (n=200), indicating that aberrant anteriorly directed migration of QL occurs frequently in the absence of Sema-2a function (Fig. 6F-H).

The DTCs of late larval stage hermaphrodites migrate on the basal surface of the hypodermis in a series of sequential steps that shape the adult gonad arms. The shape of mutant hermaphrodite gonad arms indicates that the migrating DTCs, which normally turn twice in the wild type, undergo additional turns in 9% (n=131) of *mab-20(ev574); him-5* compared to 1% (n=101) of *him-5* control hermaphrodites. There is no correlation between the body shape abnormalities and either the QL or DTC migratory defects. These results suggest that Ce-Sema-2a may be required to prevent the migration of both the QL and the DTCs beyond their normal stopping points.

mab-20 reporters are expressed during hypodermal development and male tail morphogenesis

Two different types of *mab-20* reporter constructs were made.

Table 2. Axon guidance defects of *mab-20* mutants and strains expressing ectopic *mab-20(+).*

Genotype	% misguided DA/DB axons	% defasciculated nerve cords	n
control	0	3	100
*mab-20(ev574)**	4	17	106
evIs74a[mab-20(+); rol-6(su1006)]	3	8	100

Axon guidance and nerve cord fasciculation defects are reported as percentages of animals that contain them. Strains carried the transgene array *evIs82b[evIspAC12 (unc-129^{ns}::gfp); dpy-20(+)]* in order to visualize axons and nerve cords. All strains studied also contained *him-5(e1490)* except (*).

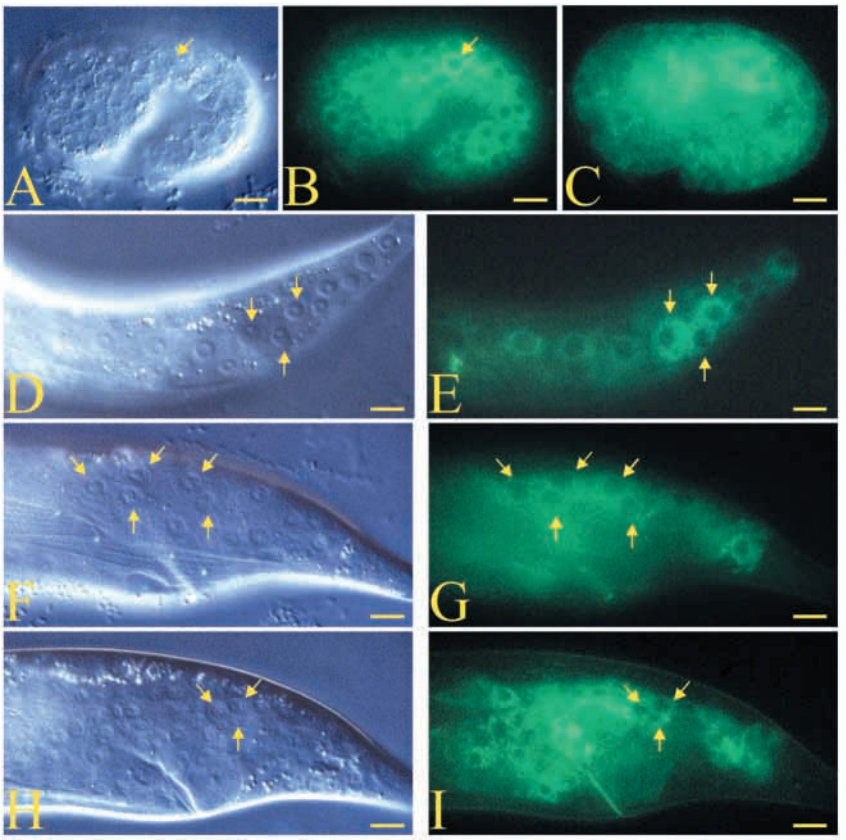

Fig. 7. Expression patterns generated from a GFP-tagged Ce-Sema-2a reporter construct. All animals shown contain the *mab-20* translational fusion reporter transgene, *evIs102a [mab-20::gfp(evpPRII.14); rol-6(su1006)]* and *him-5(e1490)*. The photomicrographs to the right are epifluorescence images of the same animals shown with DIC optics on the left. Each animal is shown in a lateral perspective with anterior to the left. (A) An embryo at the comma stage (following completion of ventral enclosure). (B) Ubiquitous expression of the *mab-20::*GFP reporter throughout the surface cells of the embryo shown in A, and in deeper focal planes (C). Arrows in A and B point to a seam cell. (D,E) A third larval-stage male at about 30 hours after hatching. Expression of *mab-20*::GFP is observed in the R(n) cells (yellow arrows indicate three examples) that give rise to the R(n).p cells and in turn, the ray precursor clusters. (F-I) An early to mid-L4 stage male at about 35 hours after hatching. The R(n).p cells (arrows in F and G) express *mab-20*::GFP, as do the ray precursor clusters (arrows in H and I point to a single cluster}, which are the R(n).p descendents and are situated in a deeper focal plane. Scale bars are 10 μm.

evpPRII.67 and *evpPRII.75* are transcriptional fusions to *gfp*, while *evpPRII.14* encodes a GFP-tagged version of Ce-Sema-2a (Fig. 2). Like the *evIs74* series of *mab-20*(+) transgene arrays (Table 1), animals transgenic for *evpPRII.14*, but not *evpPRII.67* and *evpPRII.75*, phenocopy *mab-20* mutants (data not shown).

Except for an earlier onset of GFP expression from both *evpPRII.67* and *evpPRII.75*, all reporters displayed very similar expression patterns. Embryonic GFP expression reported by *evpPRII.14* is first visible at approximately 240 minutes of development and is ubiquitous (Fig. 7), a pattern that persists until hatching. At the beginning of each larval stage, dividing seam cells express *mab-20*::GFP, as do both daughter cells in males and hermaphrodites. After the anterior daughter fuses with surrounding hyp7, *mab-20*::GFP expression is downregulated or shut off in the both daughters. Other hypodermal expression is not evident in males or hermaphrodites. Other cells that express *mab-20*::GFP in hermaphrodites include the hermaphrodite-specific neurons at the L4 stage, vulva cells A to F throughout development, the migrating distal tip cells during the L4 stage, and several unidentified neurons within the nerve ring and ventral nerve cord. Expression in males include cells in the posterior ganglia, the migrating male linker cell beginning at the L3 to L4 transition, and the same nerve ring and ventral nerve cord expression observed in hermaphrodites.

About 35 hours after hatching, mid-L3 males express *mab-20*::GFP in the 9 R(n) cells that give rise to the ray precursor clusters (Fig. 7). Interior neuronal ganglia also express lower levels of *mab-20*::GFP at this stage. At 38-40 hours, when ray papillae are just visible, the 9 R(n)s and their descendents express *mab-20*::GFP. However, the underlying neural ganglia express the same level of GFP as the ray precursors at this stage. This pattern of expression continues until adulthood.

DISCUSSION

The fundamental molecular mechanisms involved in cell shape changes, cell movements, and the spatial rearrangements of cells that generate form are only beginning to be understood. One of the first examples of a protein that regulates epithelial morphogenesis is the product of the *Drosophila decapentaplegic* (*dpp*) gene. Dpp is a member of the TGF-β superfamily of secreted ligands that is required for concerted shape changes in epithelial cells that enclose the embryo through a process known as dorsal closure (Riesgo-Escovar and Hafen, 1997). The row of epithelial cells that constitute the dorsal edge of the epithelium activates a JNK pathway that results in the expression of *dpp*. Exactly how *dpp* expression in the leader cells orchestrates a concerted elongation of the lateral epithelial cells in a dorsoventral (DV) direction is unknown. Somewhat analogous to *Drosophila* dorsal closure is ventral enclosure in *C. elegans* but, instead of relying on concerted changes in the shape of lateral hypodermal cells, ventral enclosure primarily depends on an active migration of cells on the ventral edge of the hypodermis called leader cells (Williams-Masson et al., 1997). This migration is assisted by VAB-1, which putatively acts in ventral neuroblasts to guide overlying leader cell extensions to the ventral midline (George et al., 1998). Once membrane extensions from contralateral leader cells have met at the midline, a catenin-cadherin

complex encoded by *hmp-1*, *hmp-2* and *hmr-1* is thought to fortify the contacts and enable the completion of leader cell migration (Costa et al., 1998).

An unexplored question concerning ventral enclosure and morphogenesis in general is how concerted cell movements, shape changes and spatial rearrangements of cells, all of which involve the formation and breaking of transient contacts between cells or with the ECM, are regulated. A detailed study of the phenotype of *mab-20* mutants has revealed that *C. elegans* Semaphorin-2a regulates the formation or stabilization of contacts between epithelial cells during epithelial morphogenesis. To put the morphogenetic defects of *mab-20* mutants into context, a brief review of the major morphogenetic events of *C. elegans* development is presented.

C. elegans hypodermal morphogenesis can be divided into several steps. First, several short-range migrations and rearrangements of ectoblasts produce six longitudinal rows of hypodermal cells that sit on the embryo in a dorsal-posterior locale, leaving the ventral neuroblasts uncovered (Sulston et al., 1983). Second, while the two dorsal rows of hypodermal cells intercalate, the leader cells of the ventral row of hypodermal cells initiate a migration towards the ventral midline to cover the rest of the body of the embryo in hypodermis in a process called ventral enclosure (Williams-Masson et al., 1998, 1997). It is not known how the head becomes covered with hypodermis. Third, microfilament bundles within the hypodermis align in parallel along the circumferential contour after ventral enclosure. The fourfold elongation of the embryo is mediated by the threefold contraction of these circumferential microfilaments (Priess and Hirsh, 1986). Fourth, six P cells become vulva precursor cells, some of which undergo several divisions, movements and fusions, and then evert to form a vulva by adulthood (Greenwald, 1997). Fifth, the three posterior seam cells on both sides of males undergo extra rounds of division in the third and fourth larval stages to generate the ray precursor cells (Sulston et al., 1980). Finally, an anterior-directed retraction of the entire male tail at the end of the fourth larval stage results in the formation of male tail sensory rays embedded within a cuticular fan. Except for dorsal hypodermal intercalation, head and vulva morphogenesis, and the anterior retraction of the male tail, Ce-Sema-2a is involved in each of these processes.

The earliest phenotypic trait of *mab-20* mutants is the clustering of lateral hypodermal seam cells with each other. During the longitudinal alignment of the seam cell rows, numerous migrations and rearrangements of seam cells and their precursors occur. A comparison of the seam cell positions in *mab-20* mutant embryos to the wild type suggests that migrating seam cells fail to reach their normal anteroposterior (AP) positions, resulting in the observed mutant seam cell clusters.

The next defect observed in *mab-20* mutants is the formation of ectopic contacts between non-neighboring ipsilateral ventral hypodermal cells as they move ventrally (Fig. 3H). These early ectopic contacts likely persist and are later observed as ectopic contacts between P cells after the completion of ventral enclosure (Fig. 3J). The ventral hypodermal cell defects do not appear to depend on prior defects in seam cell arrangements, since they can occur even when all of the seam cells have migrated and intercalated properly.

There are at least two classes of ventral hypodermal cells that exhibit different behaviors during enclosure. On each side there are two leader cells that extend long actin-rich membrane extensions, while the more posterior hypodermal pocket cells fail to extend substantial actin-rich processes (our observations; Williams-Masson et al., 1997). Observation of live embryos by Raich and Hardin (personal communication) suggest that pocket cells exhibit membrane extensions, but these are transient, much shorter than their leader cell counterparts, and cannot be observed by phalloidin staining. It is tempting to speculate that Ce-Sema-2a acts to limit membrane extensions from pocket cells. For example, the actin-rich extensions that emanate from the pocket cells of *mab-20* mutant embryos could represent exploratory processes that would otherwise collapse in the presence of Ce-Sema-2a (Fig. 3E-F). Instead, in the absence of Ce-Sema-2a, these exploratory processes may be free to extend and establish stable ectopic contacts to non-neighboring pocket cells. Leader cells may be unresponsive to the presence of Ce-Sema-2a and therefore extend processes in its presence or absence.

The third defect observed in *mab-20* embryos is the extrusion of internal contents from the ventral surface during embryonic elongation. Contraction of the circumferential hypodermal microfilaments presumably forces internal contents through the incompletely enclosed ventral surface of *mab-20(ev574)* embryos in a manner similar to *vab-1(e2027)* mutants. However, our results indicate that enclosure fails in these two mutants for different reasons. It is thought that VAB-1 either directly or indirectly regulates ventral neuroblast interaction with the overlying ventral hypodermis to guide the extensions of contralateral leader cells towards each other (George et al., 1998). In *vab-1(e2027)* mutants, the contralateral ventral hypodermal cells frequently fail to come together at the ventral midline, resulting in embryos that burst during elongation. Our observations show that those *vab-1(e2027)* mutants that escape lethality have no ectopic pocket cell contacts, suggesting that a disruption of neuroblast-hypodermal interaction does not necessarily result in ectopic hypodermal cell contacts. In contrast to *vab-1* mutants, the data presented here suggest that Ce-Sema-2a prevents ectopic contacts between ventral hypodermal cells during enclosure. Thus, *mab-20* mutants most likely burst from the ventral side during elongation because abnormal pocket cell contacts either sterically hinder pocket closure or weaken the contacts formed between the contralateral pocket cells at the ventral midline.

Those *mab-20* mutant embryos that escape lethality frequently develop severe bulges and constrictions during embryonic elongation. Body wall bulges are always coincident with circumferentially misaligned microfilaments contained within the clustered seam cells of *mab-20* mutants. This observation raises two obvious and related questions. First, do misaligned microfilaments cause the bulge or do body wall bulges disrupt the alignment of microfilaments? Several lines of evidence support the former hypothesis. (1) Microfilament alignment is a prerequisite to elongation (Priess and Hirsh, 1986), and the bulges are only observed in mutants well into elongation and past the twofold stage. (2) Single seam cells containing misaligned microfilaments are observed without a corresponding bulge in the body wall (Roy, 1999), but bulges are never observed without a corresponding cluster of seam cells containing misaligned microfilaments. (3) Microfilament arrays are often U-shaped within the clustered seam cells,

extending back toward the same side of the animal as the side of their origin. It is easy to imagine how the contraction of these U-shaped filaments results in the associated bulge. Together, these results strongly suggest that misaligned microfilaments cause body wall bulging and not vice versa.

A second question is whether microfilaments are misaligned because of the ectopic contacts of the seam cells in which they are contained, or because their alignment depends on a global mechanism or cue that is disrupted in *mab-20* mutants. The latter hypothesis is not as likely since (1) there are no obvious alterations in the axes of *mab-20* mutants and (2) microfilament alignment is never aberrant in dorsal hypodermis and rarely deviates from normal in the ventral hypodermis. Instead, we hypothesize that as a secondary consequence of not properly intercalating within the seam cell queue, the DV and AP axes of clustered seam cells can become skewed. This in turn skews unknown determinants of microfilament polarity and results in a corresponding misalignment of microfilaments prior to elongation.

The last observed morphogenetic defect in *mab-20* mutants is the fusion of normally distinct sensory rays of the male tail. In all *mab-20* alleles, an exact correlation is found between those ray precursor clusters that make ectopic contacts and those rays that later fuse, suggesting a causal relationship (our observations; Baird et al., 1991; Chow and Emmons, 1994). Intervening hyp7 prevents lasting contacts between neighboring ray precursor clusters, a process that fails in *mab-20* mutants. A subtle question that arises is whether the focus of Sema-2a in the male tail is the regulation of contact formation between hyp7 and the R(n).ps or between neighboring clusters. Since hyp7 contacts the dorsal and ventral sides of the R(n)s before they give rise to the ray precursors, it is difficult to imagine anything but a passive role for hyp7 in maintaining distinct ray precursor clusters as they are born. Thus, it is more likely that Sema-2a regulates contact formation between neighboring precursor clusters, possibly by preventing membrane extension between clusters that would otherwise result in stable contacts between clusters and consequent ray fusions.

The role of Ce-Sema-2a in axon guidance

The errors in nerve cord fasciculation and circumferential pioneer axon guidance in *mab-20* mutants could be secondary defects that result from the aberrant positioning of cues from a disorganized hypodermis. Alternatively, these cells may require Ce-Sema-2a directly as a guidance cue, an expectation that is based on one known function of the vertebrate semaphorins. The lack of highly penetrant axon guidance and cell migration defects in *mab-20* mutants may reflect a function in axon guidance that is redundant with the other two semaphorin genes present in the *C. elegans* genome (D1037.2 and Y54E5B.1). Our recent recovery of mutations in these genes (P. J. R., V. Ginzburg and J. G. C., unpublished results) should allow us to test this possibility. The characterization of mutants defective in putative signaling components downstream of Sema-2a, such as a Ce-Sema-2a receptor, may also enable us to test whether Ce-Sema-2a directly guides migrations (R. Ikegami and J. G. C., unpublished results).

A model for Ce-Sema-2a activity

We show here for the first time that a member of the semaphorin family regulates both epithelial morphogenesis and the migrations of cells, including epidermal cells, the QL neuroblast and the distal tip cells. In addition, Ce-Sema-2a plays a role in guiding DA and DB pioneer axons. As each of these cells and axons migrate towards their target destination, they must transiently establish contacts to neighboring cells and the ECM via membrane extensions. It is through the modulation of the cytoskeletal network within these membrane extensions that cues such as SEMA3A can guide migrations (Fan and Raper, 1995). One simple model that explains the ectopic hypodermal cell contacts and the errors in cell and axon guidance in *mab-20* mutants is that, akin to SEMA3A, Ce-Sema-2a functions to prevent or repel cellular extensions of actin-rich exploratory processes. In the absence of functional Ce-Sema-2a, the QL neuroblast and the distal tip cells migrate beyond their normal stopping points, the DA and DB axons fail to restrict exploration, and epithelial pocket cells, seam cells and ray precursor clusters fail to restrict inappropriate adhesive contacts with each other during morphogenesis.

mab-20 reporters are expressed nearly ubiquitously during mid-embryogenesis and male tail morphogenesis, yet many migrations and cell rearrangements in *mab-20* mutants are normal. The ability of a cell to respond to Sema-2a must therefore be controlled by the expression of a Sema-2a receptor, a co-factor or downstream signaling components, rather than by the tight spatiotemporal control of Ce-Sema-2a production. MAB-26 is a candidate for a regulated element of the Ce-Sema-2a pathway since *mab-26* mutants share many of the phenotypic traits of *mab-20* mutants and do not appear to significantly enhance the *mab-20* null allele (Roy, 1999). Sema-2a may be a global regulator of cell-cell interactions and any cell with the ability to receive and transduce the Sema-2a signal may have access to such regulation.

We thank U. Tepass and D. Merz for critically reading the manuscript, A. Colavita for providing the *unc-129*^{ns} reporter lines, T. Stiernagle of the Caenorhabditis Genetics Center, which is funded by the NIH National Center for Research Resources, for providing strains, M. Couto and R. Waterston for providing the MH27 antibody, M. Labouesse for providing anti-LIN-26, A. Fire for providing the GFP reporter vectors, J. Dennis, A. Spence and M. Perry for many helpful discussions, and all members of the Culotti laboratory for comments. This work was supported by a grant from the Canadian MRC to J. G. C. and a Canadian NSERC postgraduate scholarship to P. J. R.

REFERENCES

Altschul, S. F., Gish, W., Miller, W., Myers, E. W. and Lipman, D. J. (1990). Basic local alignment search tool. *J. Mol. Biol.* **215**, 403-410.

Bagnard, D., Lohrum, M., Uziel, D., Puschel, A. W. and Boiz, J. (1998). Semaphorins act as attractive and repulsive guidance signals during the development of cortical projections. *Development* **125**, 5043-5053.

Baird, S. E., Fitch, D. H., Kassem, I. A. A. and Emmons, S. W. (1991). Pattern formation in the nematode epidermis: determination of the peripheral sense organs in the *C. elegans* male tail. *Development* **113**, 515-526.

Behar, O., Golden, J. A., Mashima, H., Schoen, F. J. and Fishman, M. C. (1996). Semaphorin III is needed for normal patterning and growth of nerves, bones and heart. *Nature* **383**, 525-528.

Carlier, M. F. (1998). Control of actin dynamics. *Curr. Opin. Cell Biol.* **10**, 45-51.

Chan, S. S-Y., Zheng H., Su M-W., Wilk, R., Killeen, M. T., Hedgecock, E. M. and Culotti, J. G. (1996). UNC-40, a *C. elegans* homolog of DCC

(deleted in colorectal cancer), is required in motile cells responding to UNC-6 netrin cues. *Cell* **87**, 187-195.

Chow, K. L. and Emmons, S. W. (1994). Hom-C/Hox genes and four interacting loci determine the morphogenetic properties of single cells in the nematode male tail. *Development* **120**, 2579-2593.

Colavita, A. and Culotti, J. G. (1998). Suppressors of ectopic UNC-5 growth cone steering identify eight genes involved in axon guidance in *Caenorhabditis elegans*. *Dev. Biol.* **194**, 72-85.

Colavita, A., Krishna, S., Zheng, H., Padgett, R. W. and Culotii, J. G. (1998). Pioneer axon guidance by UNC-129, a *C. elegans* TGB-β. *Science* **281**, 706-709.

Costa, M., Raich, W., Agbunag, C., Leung, B., Hardin, J. and Priess, J. R. (1998). A putative catenin-cadherin system mediates morphogenesis of the Caenorhabditis elegans embryo. *J. Cell Biol.* **141**, 297-308.

de la Torre, J. R., Hopker, V. H., Ming, G-L., Poo, M-m., Tessier-Lavigne, M., Hemmati-Brivanlou, A. and Holt, C. E. (1997). Turning of retinal growth cones in a Netrin-1 gradient mediated by the Netrin receptor DCC. *Neuron* **19**, 1211-1224.

Eickholt, B. J., Mackenzie, S. L., Graham, A., Walsh, F. S. and Doherty, P. (1999). Evidence for collapsin-1 functioning in the control of neural crest migration in both trunk and hindbrain regions. *Development* **126**, 2181-2189.

Fan, J. and Raper, J. A. (1995). Localized collapsing cues can steer growth cones without inducing their full collapse. *Neuron* **14**, 263-274.

Finney, M. and Ruvkun, G. (1990). The *unc-86* gene product couples cell lineage and cell identity in *C. elegans*. *Cell* **63**, 895-905.

Francis, R. and Waterston, R. H. (1991). Muscle cell attachment in *Caenorhabditis elegans*. *J. Cell Biol.* **114**, 465-479.

Frohman, M. A., Dush, M. K. and Martin, G. R. (1988). Rapid production of full-length cDNAs from rare transcripts:amplification using a single gene-specific oligonucleotide primer. *Proc. Natl. Acad. Sci. USA* **85**, 8998-9002.

George, S. E., Simokat, K., Hardin, J. and Chisholm, A. D. (1998). The *VAB-1* Eph receptor tyrosine kinase functions in neural and epithelial morphogenesis in *C. elegans*. *Cell* **92**, 633-643.

Greenwald, I. (1997). In *C. elegans II*. (ed. D. L. Riddle, T. Blumenthal, B. J. Meyer and J. R. Priess), pp. 519-541. Cold Spring Harbor, NY: Cold Spring Harbor Laboratory Press.

He Z. and Tessier-Lavigne, M. (1997). Neuropilin is a receptor for the axonal chemorepellent Semaphorin III. *Cell* **90**, 739-751.

Hedgecock, E. M., Culotti, J. G. and Hall, D. H. (1990). The *unc-5*, *unc-6*, and *unc-40* genes guide circumferential migrations of pioneer axons and mesodermal cells on the epidermis in *C. elegans*. *Neuron* **2**, 61-85.

Kitsukawa, T., Shimono, A., Kawakami, A., Kondoh, H. and Fujisawa, H. (1995). Overexpression of a membrane protein, neuropilin, in chimeric mice causes anomalies in the cardiovascular system, nervous system and limbs. *Development* **121**, 4309-4318.

Kolodkin, A. L., Matthes, D. J. and Goodman, C. S. (1993). The semaphorin genes encode a family of transmembrane and secreted growth cone guidance molecules. *Cell* **75**, 1389-1399.

Kolodkin, A. L., Matthes, D. J., O'Connor, T. P., Patel, N. H., Admon, A., Bentley, D. and Goodman, C. S. (1992). Fasciclin IV: Sequence, expression and function during growth cone guidance in the grasshopper embryo. *Neuron* **9**, 831-845.

Krause, M. and Hirsh, D. (1987). A trans-spliced leader sequence on actin mRNA in *C. elegans*. *Cell* **49**, 753-761.

Labouesse, M., Hartwieg, E. and Horvitz, H. R. (1996). The *Caenorhabditis elegans* LIN-26 protein is required to specify and/or maintain all non-neuronal ectodermal cell fates. *Development* **122**, 2579-2588.

Leung-Hagesteijn, C., Spence, A. M., Stern, B. D., Zhou, Y., Su, M-W., Hedgecock, E. M. and Culotti, J. G. (1992). UNC-5, a transmembrane protein with immunoglobulin and thrombospodin type 1 domains, guides cell and pioneer axon migrations in *C. elegans*. *Cell* **71**, 289-299.

Mello, C. C. and Fire, A. (1995). DNA transformation in *Caenorhabditis elegans;* modern biological analysis of an organism. (ed. H. F. Epstein and D. C. Shakes). *Methods in Cell Biology* **48**, 452-482.

Podbilewicz, B. and White, J. G. (1994). Cell fusions in the developing epithelia of *C. elegans*. *Dev. Biol.* **161**, 408-424.

Priess, J. R. and Hirsh, D. I. (1986). *Caenorhabditis elegans* morphogenesis: The role of the cytoskeleton in elongation of the embryo. *Dev. Biol.* **117**, 156-173.

Riesgo-Escovar, J. R. and Hafen, E. (1997). Drosophila Jun kinase regulates expression of decapentaplegic via the ETS-domain protein Aop and the AP-1 transcription factor DJun during dorsal closure. *Genes Dev.* **11**, 1717-1727.

Roy, P. J. (1999). The cloning and characterization of two semaphorin genes *in C. elegans*. Ph.D. Thesis, University of Toronto.

Sambrook, J., Fritsch, E. F. and Maniatis, T. (1989). *Molecular Cloning: a Laboratory Manual*. Cold Spring Harbor, New York: Cold Spring Harbor Laboratory.

Schnabel, R., Hutter, H., Moerman, D. and Schnabel, H. (1997). Assessing normal embryogenesis in Caenorhabditis elegans using a 4D microscope: Variability of development and regional specification. *Dev. Biol.* **184**, 234-265.

Semaphorin Nomenclature Committee (1999). Unified nomenclature for the semaphorins/collapsins. *Cell* **28**, 551-552.

Soker, S., Takashima, S., Miao, H. Q., Neufeld, G. and Kladsbrun, M. (1998). Neuropilin-1 is expressed by endothelial and tumour cells as an isoform-specific receptor for vascular endothelial growth factor. *Cell* **92**, 735-745.

Song, H-j., Ming, G-l., He, Z., Lehmann, M., McKerracher, L., Tessier-Lavigne, M. and Poo, M-m. (1998). Conversion of neuronal growth cone responses from repulsion to attraction by cyclic nucleotides. *Science* **281**, 1515-1518.

Sulston, J. E. and Horvitz, H. R. (1977). Postembryonic cell lineages of the nematode *Caenorhabditis elegans*. *Dev. Biol.* **56**, 110-156.

Sulston, J. E., Albertson, D. G. and Thomson, J. N. (1980). The *Caenorhabditis elegans* male: Postembryonic development of nongonadal structures. *Dev. Biol.* **78**, 542-576.

Sulston, J. E., Schierenberg, E., White, J. G. and Thomson, J. N. (1983). The embryonic cell lineage of the nematode *Caenorhabditis elegans*. *Dev. Biol.* **100**, 64-119.

Tanaka, E. and Sabry, J. (1995). Making the connection: Cytoskeletal rearrangements during growth cone guidance. *Cell* **83**, 171-176.

Williams-Masson, E. M., Malik, A. N. and Hardin, J. (1997). An actin-mediated two-step mechanism is required for ventral enclosure of the *C. elegans* hypodermis. *Development* **124**, 2889-2901.

Williams-Masson, E. M., Hied, P. J., Lavin, C. A. and Hardin, J. (1998). The cellular mechanism of epithelial rearrangement during morphogenesis of *the Caenorhabditis elegans* dorsal hypodermis. *Dev. Biol.* **204**, 263-276.

Winberg, M. L., Mitchell, K. J. and Goodman, C. S. (1998). Genetic analysis of the mechanisms controlling target selection: Complementary and combinatorial functions of Netrins, Semaphorins and IgCAMs. *Cell* **93**, 581-591.

Wong, J. T., Yu, W. T. and O'Connor, T. P. (1997). Transmembrane grasshopper Semaphorin I promotes axon outgrowth in vivo. *Development* **124**, 3597-3607.

Wood, B. (1988). *In* "The Nematode *Caenorhabditis elegans*". (B. Wood and the community *of C. elegans* researchers, Eds.) Cold Spring Harbor Laboratory Press. Cold Spring Harbor, NY.

Yu, H-H, Araj, H. H., Rallis, S. A. and Kolodkin, A. L. (1998). The transmembrane Semaphorin Sema I is required in *Drosophila* for embryonic motor and CNS axon guidance. *Neuron* **20**, 207-220.

Zwaal, R. R., Broeks, A., van Meurs, J., Groenen, T. M. and Plasterk, R. H. (1993). Target-selected gene inactivation in *Caenorhabditis elegans* by using a frozen transposon insertion mutant bank. *Proc. Natl. Acad. Sci. U.S.A.* **90**, 7431-7435.